

First-principles study of ground state properties of ZrH_2

Peng Zhang,^{1,2} Bao-Tian Wang,^{3,2} Chao-Hui He,¹ and Ping Zhang^{2,4,*}

¹*Department of Nuclear Science and Technology,*

Xi'an Jiaotong University, Xi'an 710049, People's Republic of China

²*LCP, Institute of Applied Physics and Computational Mathematics,*

Beijing 100088, People's Republic of China

³*Institute of Theoretical Physics and Department of Physics,*

Shanxi University, Taiyuan 030006, People's Republic of China

⁴*Center for Applied Physics and Technology,*

Peking University, Beijing 100871, People's Republic of China

Abstract

Structural, mechanical, electronic, and thermodynamic properties of fluorite and tetragonal phases of ZrH_2 are systematically studied by employing the density functional theory within generalized gradient approximation. The existence of the bistable structure for ZrH_2 is mainly due to the tetragonal distortions. And our calculated lattice constants for the stable face-centered tetragonal (fct) phase with $c/a=0.885$ are consistent well with experiments. Through calculating elastic constants, the mechanically unstable characters of face-centered cubic (fcc) phase and fct structure with $c/a=1.111$ are predicted. As for fct0.885 structure, our calculated elastic constants explicitly indicate that it is mechanically stable. Elastic moduli, Poisson's ratio, and Debye temperature are derived from elastic constants. After analyzing total and partial densities of states and valence electron charge distribution, we conclude that the Zr–H bonds in ZrH_2 exhibit weak covalent feature. But the ionic property is evident with about 1.5 electrons transferring from each Zr atom to H. Phonon spectrum results indicate that fct0.885 and fct1.111 structures are dynamically stable, while the fcc structure is unstable.

PACS numbers: 61.50.Ah, 62.20.Dc, 71.15.Mb, 63.20.dk

*Author to whom correspondence should be addressed. E-mail: zhang_ping@iapcm.ac.cn

I. INTRODUCTION

Many transition metals react readily with hydrogen to form stable metal hydrides [1]. The common metal hydrides are technologically attractive materials due to their ability to store high densities of hydrogen safely. In the case of zirconium hydrides, another appealing interest arises in nuclear industry, essentially used as a neutron moderator [2] and fuel rod cladding materials [3] in nuclear reactors. Additionally, in the fusion technology applications, zirconium hydrides are unavoidably precipitated in the excess of the hydrogen solubility, which may adversely affect several mechanical and thermal properties in some crystal orientations [4] involving different stable and metastable hydride phases which may lead to a significant embrittlement. Furthermore, zirconium hydrides are also served as a part of the promising new type of actinide hydride fuels, such as U-(Th-Np-Am)-Zr-H [5]. Consequently, great attentions are needed to focus on the basic scientific research of zirconium hydrides.

Since 1952, there has occurred in literature large amounts of experimental investigations on zirconium hydrides. The electronic structures of ZrH_x ($1.63 \leq x \leq 1.94$) was studied using photoelectron spectroscopy and synchrotron radiation [6], where the Jahn-Teller effect is demonstrated by the changes of electrons occupation at the Fermi level. An assessed H-Zr phase diagram was successfully constructed by Zuzek *et al.* [7] in 1990. And the transition between the cubic and the tetragonal phases has been suggested by Ducastelle *et al.* [8] to be of Jahn-Teller type too. From theoretical point of view, the phase transition between cubic and tetragonal phases has been investigated by Switendick [9], where the non-self-consistent augmented plane wave (APW) method was employed. Most importantly, the study of the electronic structure and energetics for the tetragonal distortion in ZrH_2 has been extensively performed. Using the pseudopotential method with both local density approximation (LDA) and general gradient approximation (GGA), Ackland [10] obtained a double minimum in the energy surface, one minimum for $c/a < 1$ and the other for $c/a > 1$ with an energy barrier in between of roughly 0.1 eV. But the ground state for $c/a > 1$ was in clear disagreement with the experimental data [11–16]. Recently, Wolf and Herzig [17] and Quijano *et al.* [18] studied the accurate total energy and the electronic structure characteristic of ZrH_2 by using LDA and GGA, respectively, within the full potential linear augmented plane wave (FP-LAPW) method. Both of these works obtained the correct ground state for $c/a < 1$ and made a clear

explanation of the cubic to tetragonal distortion.

However, despite the abundant theoretical and experimental research on zirconium hydrides, relatively little is known regarding their chemical bonding nature, mechanical properties, and the phonon dispersions. Until now, the elastic properties, which relate to various fundamental solid state properties such as interatomic potentials, equation of states, phonon spectra, and thermodynamical properties are nearly unknown for ZrH_2 . Moreover, although the electronic properties as well as the chemical bonding in zirconium dihydride have been calculated [17], the study of the bonding nature of Zr-H involving its mixed ionic/covalent character is still lacking. As a consequence, these facts inhibit deep understanding of the zirconium dihydride. Motivated by these observations, in this paper, we present a first-principles study by calculating the structural, electronic, mechanical, and thermodynamical properties of zirconium dihydride. Our calculated results show that the bistable structure of ZrH_2 is the fct phase at $c/a=0.885$ and $c/a=1.111$, respectively. The mechanical and dynamical stability of fct and fcc phases of ZrH_2 are carefully analyzed. In addition, through Bader analysis [19, 20] we find that about 1.5 electrons transfer from each Zr atom to H atom for ZrH_2 .

II. COMPUTATIONAL METHOD

Our total energy calculations are self-consistently carried out using density functional theory (DFT) as implemented in Vienna ab initio simulation package (VASP) [21], which is based on pseudopotentials and plane wave basis functions. All electron projected augmented wave (PAW) method of Blöchl [22] is applied in VASP with the frozen core approximation. The generalized gradient approximation (GGA) introduced by Perdew, Burke, and Ernzerhof (PBE) [23] is employed to evaluate the electron exchange and correlation potential. Zirconium $4s^2 4p^6 4d^2 5s^2$ and hydrogen $1s^1$ electrons are treated as valence electrons. The integration over the Brillouin Zone (BZ) is performed with a grid of special k point-mesh determined according to the Monkhorst-Pack scheme [24]. After convergence test, $12 \times 12 \times 12$ k point-mesh is chosen to make sure the total energy difference less than 1 meV per primitive cell. When exploring the electronic structure, a finer k point-mesh $24 \times 24 \times 24$ is preferred to generate a high quality charge density. The expansion of the valence electron plane wave functions can be truncated at the cutoff energy of 650 eV, which has been tested to be fully

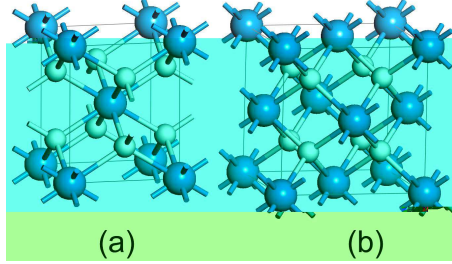


FIG. 1: Tetragonal unit cell in space group $I4/mmm$ (a) and cubic unit cell for ZrH_2 in space group $Fm\bar{3}m$ (b) with larger cyan spheres for Zr atoms and the smaller white H.

converged with respect to total energy. Relaxation procedures at ground state are carried out according to the Methfessel-Paxton scheme [25] with a smearing width of 0.1 eV. The geometry relaxation is considered to be completed when the Hellmann-Feynman forces on all atoms were less than 0.001 eV/\AA . And the accurate total energy calculations are performed by means of the linear tetrahedron method with the Blöchl's corrections [26]. The self-consistent convergence of the total energy calculation is set to 10^{-6} eV .

III. RESULTS

A. Atomic structure and mechanical properties

At ambient condition, the stable zirconium dihydride crystallizes in a fct structure with space group $I4/mmm$ (No. 139). In its unit cell, there are two ZrH_2 formula units with Zr and H atoms in $2a:(0,0,0)$ and $4d:(0, \frac{1}{2}, \frac{1}{4})$ sites, respectively [see Fig. 1(a)]. Each Zr atom is surrounded by eight H atoms forming a tetragonal and each H connects with four Zr atoms to build a tetrahedron. The present optimized equilibrium lattice parameters (a and c) obtained by fitting the energy-volume data in the third-order Birch-Murnaghan equation of states (EOS) [27] are 5.030 \AA and 4.414 \AA (see Table I), in good agreement with the experimental values. In addition, the fcc fluorite type structure with space group $Fm\bar{3}m$ (No. 225) is considered as the metastable phase for ZrH_2 . The cubic unit cell is composed of four ZrH_2 formula units with the Zr and H atoms in $4a:(0,0,0)$ and $8c:(\frac{1}{4}, \frac{1}{4}, \frac{1}{4})$ sites, respectively [see Fig. 1(b)]. Here, each Zr atom is surrounded by eight H atoms forming a cube and each H atom connects with four Zr atoms to build a tetrahedron. Our optimized equilibrium lattice constant a for fcc ZrH_2 is 4.823 \AA . This value, although no experimental

TABLE I: Calculated lattice constants, bulk modulus B_0 , and pressure derivative of the bulk modulus B'_0 at ground state from EOS fitting. For comparison, available experimental values and other theoretical results are also listed.

Compounds	Property	Present work	Previous calculation	Experiment
fcc ZrH ₂	a_0 (Å)	4.823	4.817 ^a , 4.804 ^b	-
	B_0 (GPa)	133	136 ^a , 152 ^b	-
	B'_0	4.01	-	-
fct ZrH ₂	a_0 (Å)	5.030	5.021 ^a , 5.008 ^b , 5.000 ^c	4.985 ^d , 4.975 ^e , 4.982 ^f
	c_0 (Å)	4.414	4.432 ^a , 4.419 ^b , 4.450 ^c	4.430 ^d , 4.447 ^e , 4.449 ^f
	B_0 (GPa)	127	-	-
	B'_0	3.62	-	-

^a Reference [18], ^b Reference[17], ^c Reference [10], ^d Reference [11], ^e Reference[16], ^f Reference [12].

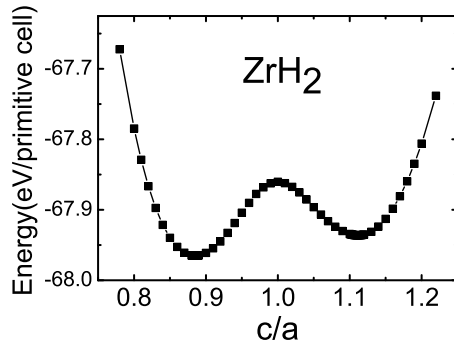


FIG. 2: Total energy as a function of the c/a ratio in the fct phase for ZrH₂.

structural values are available for comparison, is in good agreement with previous theoretical work in the literature (see Table I).

In present study, the stability of ZrH₂ has been investigated by calculating the total energy as a function of c/a at the optimized constant volume of fcc structure, as illustrated in Fig. 2. The energy curve displays two local minima, one with $c/a < 1$ (0.885) and the other with $c/a > 1$ (1.111). The minimum at $c/a = 0.885$ has the lowest energy and corresponds to fct phase observed experimentally. The fct-fcc structure energy barrier obtained from this calculation is 0.1048 eV, in good agreement with the Ackland's results [10] but much larger than the FP-LAPW calculation results [17, 18].

TABLE II: The strain combinations in the strain tensor [Eq. (1)] to calculate the elastic constants of cubic and tetragonal ZrH₂.

Phase Strain Parameters (unlisted $e_i=0$)			$\Delta E/V_0$ in $O(\delta^2)$
fcc	ϵ^1	$e_1=e_2=e_3=\delta$	$(\frac{3}{2}C_{11} + 3C_{12})\delta^2$
	ϵ^2	$e_1=e_2=\delta$	$(C_{11} + C_{12})\delta^2$
	ϵ^3	$e_4=e_5=e_6=\delta$	$\frac{3}{2}C_{44}\delta^2$
fct	ϵ^1	$e_1=e_2=e_3=\delta$	$(C_{11} + C_{12} + 2C_{13} + \frac{1}{2}C_{33})\delta^2$
	ϵ^2	$e_1=e_3=\delta$	$\frac{1}{2}(C_{11} + 2C_{13} + C_{33})\delta^2$
	ϵ^3	$e_1=e_2=\delta$	$(C_{11} + C_{12})\delta^2$
	ϵ^4	$e_3=\delta$	$\frac{1}{2}C_{33}\delta^2$
	ϵ^5	$e_4=e_5=\delta$	$C_{44}\delta^2$
	ϵ^6	$e_6=\delta$	$\frac{1}{2}C_{66}\delta^2$

Elastic constants can measure the resistance and mechanical features of crystal to external stress or pressure, thus may evaluate the stability of crystals against elastic deformation. For small strain ϵ , Hooke's law is valid. Therefore, we can enforce it onto the equilibrium lattice, determine the resulting change in the total energy, and from this information deduce the elastic constants. The crystal total energy $E(V, \epsilon)$ can be expanded as a Taylor series [28],

$$E(V, \epsilon) = E(V_0, 0) + V_0 \sum_{i=1}^6 \sigma_i e_i + \frac{V_0}{2} \sum_{i,j=1}^6 C_{ij} e_i e_j + O(\{e_i^3\}), \quad (1)$$

where $E(V_0, 0)$ is the energy of the unstrained system with the equilibrium volume V_0 , ϵ is the strain tensor which has matrix elements ϵ_{ij} ($i, j=1, 2, \text{ and } 3$) defined by

$$\epsilon_{ij} = \begin{pmatrix} e_1 & \frac{e_6}{2} & \frac{e_5}{2} \\ \frac{e_6}{2} & e_2 & \frac{e_4}{2} \\ \frac{e_5}{2} & \frac{e_4}{2} & e_3 \end{pmatrix}, \quad (2)$$

and C_{ij} are the elastic constants. Such a strain transforms the three lattice vectors defining the unstrained Bravais lattice $\{\mathbf{a}_k, k=1, 2, \text{ and } 3\}$ to the strained vectors $\{\mathbf{a}'_k\}$ [29] as defined by

$$\mathbf{a}'_k = (\mathbf{I} + \epsilon)\mathbf{a}_k, \quad (3)$$

TABLE III: Calculated elastic constants in units of GPa for ZrH₂ at zero pressure.

Phase	C_{11}	C_{12}	C_{44}	C_{13}	C_{33}	C_{66}
fcc	82.6	159.7	-19.5			
fct0.885	165.6	140.9	30.5	106.8	145.5	60.6
fct1.111	125.7	145.5	30.9	115.0	190.6	42.0

where \mathbf{I} is a unit 3×3 matrix. Each lattice vector \mathbf{a}_k or \mathbf{a}'_k is a 3×1 matrix.

For the cubic phase, there are three independent elastic constants, i.e., C_{11} , C_{12} , and C_{44} , which can be calculated through a proper choice of the set of strains $\{e_i, i = 1, \dots, 6\}$ (see Table II). As for the fct phase, the six independent elastic constants, i.e., C_{11} , C_{12} , C_{13} , C_{33} , C_{44} , and C_{66} , can be obtained from six different strains listed in Table II. To avoid the influence of high order terms on the estimated elastic constants, we have used very small strains, i.e. within $\pm 1.5\%$. Thus, in our calculations the strain amplitude δ is varied in steps of 0.006 from $\delta = -0.036$ to 0.036. And the total energies $E(V, \delta)$ at these strain steps are calculated and fitted through the strains with the corresponding parabolic equations of $\Delta E/V_0$ to yield the required second-order elastic constants.

Our calculated elastic constants for fcc ZrH₂ and fct ZrH₂ at $c/a=0.885$ and $c/a=1.111$ are collected in Table III. Obviously, fct ZrH₂ at $c/a=0.885$ is mechanically stable due to the fact that its elastic constants satisfy the following mechanical stability criteria [30] of tetragonal structure:

$$\begin{aligned}
 &C_{11} > 0, C_{33} > 0, C_{44} > 0, C_{66} > 0, \\
 &(C_{11} - C_{12}) > 0, (C_{11} + C_{33} - 2C_{13}) > 0, \\
 &[2(C_{11} + C_{12}) + C_{33} + 4C_{13}] > 0.
 \end{aligned} \tag{4}$$

Nevertheless, the fct phase at $c/a=1.111$ is mechanically unstable in light of the fact that C_{11} is smaller than C_{12} . As for the fcc structure of ZrH₂, it is also mechanically unstable because of the fact that its elastic constants cannot meet the following mechanical stability criteria [30] of cubic structure:

$$C_{11} > 0, C_{44} > 0, C_{11} > |C_{12}|, (C_{11} + 2C_{12}) > 0. \tag{5}$$

After obtaining elastic constants, bulk modulus B and shear modulus G for fct phase of ZrH₂ at $c/a=0.885$ can be calculated from the Voigt-Reuss-Hill (VRH) approximations

TABLE IV: Calculated bulk modulus, shear modulus, Young’s modulus, Poisson’s ratio, density, transverse sound velocity, longitudinal sound velocity, average sound velocity, and Debye temperature of the fct phase of ZrH₂ at $c/a=0.885$.

$B(\text{GPa})$	$G(\text{GPa})$	$E(\text{GPa})$	ν	$\rho(\text{g/cm}^3)$	$v_t(\text{km/s})$	$v_l(\text{km/s})$	$v_m(\text{km/s})$	$\theta_D(\text{K})$
130	29	80	0.397	5.5201	2.2823	5.5197	2.5825	364.9

[31–33]. Then the Young’s modulus E and Poisson’s ratio ν are calculated through $E = 9BG/(3B + G)$ and $\nu = (3B - 2G)/[2(3B + G)]$. The Debye temperature (θ_D) is obtained using the relation [34]

$$\theta_D = \frac{h}{k_B} \left[\frac{3n}{4\pi} \left(\frac{N_A \rho}{M} \right) \right]^{1/3} v_m, \quad (6)$$

where h and k_B are Planck’s and Boltzmann’s constants, respectively, N_A is Avogadro’s number, ρ is the density, M is the molecular weight, n is the number of atoms in the molecule, and v_m is the average wave velocity. The average wave velocity in the polycrystalline materials is approximately given as

$$v_m = \left[\frac{1}{3} \left(\frac{2}{v_t^3} + \frac{1}{v_l^3} \right) \right]^{-1/3}, \quad (7)$$

where $v_t = \sqrt{G/\rho}$ and $v_l = \sqrt{(3B + 4G)/3\rho}$ are the transverse and longitudinal elastic wave velocity of the polycrystalline materials, respectively.

All the calculated results for fct0.885 are collected in Table IV. Results of fcc and fct1.111 can not be obtained due to their mechanically unstable nature. Note that we have also calculated the bulk modulus B by EOS fitting. The derived bulk modulus for fct0.885 turns out to be very close to the one obtained from the above VRH approximation, which again indicates that our calculations are consistent and reliable. It is well known that the shear modulus G represents the resistance to plastic deformation, while the bulk modulus B can represent the resistance to fracture. A high (low) B/G value is responsible for the ductility (brittleness) of polycrystalline materials. The critical value to separate ductile and brittle materials is about 1.75. Using the calculated values of bulk modulus B and shear modulus G for fct0.885, the B/G value of 4.48 can be obtained. For element Zr, the B/G value of 2.63 can be derived from the elastic data in Ref. [35]. Therefore, fct phase of ZrH₂ is rather ductile and its ductility is more predominant than that of element Zr. As for the Poisson’s

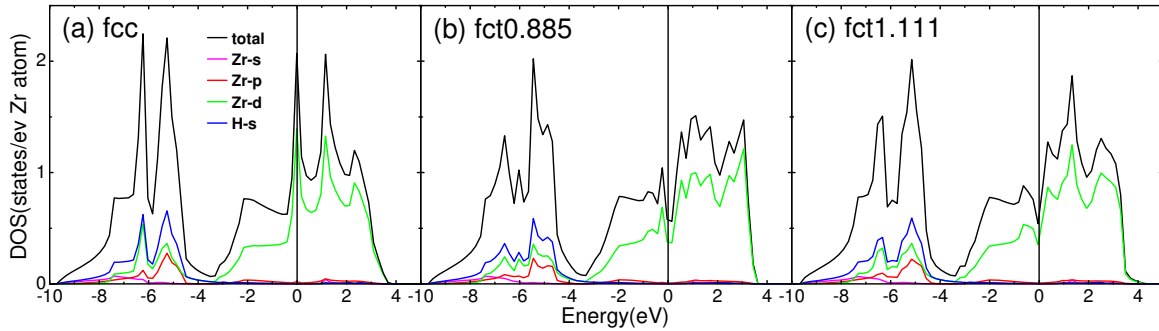


FIG. 3: Total and orbital-resolved local densities of states for (a) fcc, (b) fct0.885, and (c) fct1.111 structures of ZrH_2 . The Fermi energy level is set at zero.

ratio, the value is well within the range from 0.25 to 0.45 for typical metals. Unfortunately, no reliable experimental and theoretical results concerning on the mechanical properties in the literature are available for comparison. We hope that our calculated elastic constants and elastic moduli can be illustrative in the realistic application of the mechanical data for ZrH_2 .

B. Electronic structure and charge distribution

Basically, all the macroscopical properties of materials, such as hardness, elasticity, and conductivity, originate from their electronic structure properties as well as the nature of the chemical bonding. Therefore, it is necessary to perform the electronic structure analysis of ZrH_2 . The calculated total densities of states (DOS) and the orbital-resolved partial densities of states (PDOS) of fcc ZrH_2 , fct ZrH_2 at $c/a=0.885$ and $c/a=1.111$, are shown in Fig. 3. Wholly, the occupation properties of ZrH_2 in fct and fcc phases are similar. The pseudogap below the Fermi level, located at around -3.5 eV, for all three systems can be observed. The energy region below the pseudogap has predominant feature of hybridization for H $1s$ orbital and Zr $4d$ and Zr $4p$ orbitals. States in this region have critical contribution to the Zr-H and H-H bonding state. However, from the pseudogap to the Fermi level, H $1s$ states contribute very little to the total DOS, while the Zr $4d$ states dominate in this energy range. The fact that the DOS occupation has obvious sharp peak at the Fermi level for fcc ZrH_2 implies that the cubic phase should be unstable. In contrast, a strong reduction in the DOS at the Fermi level is observed in the two fct structures. This evident difference between fcc and fct phase

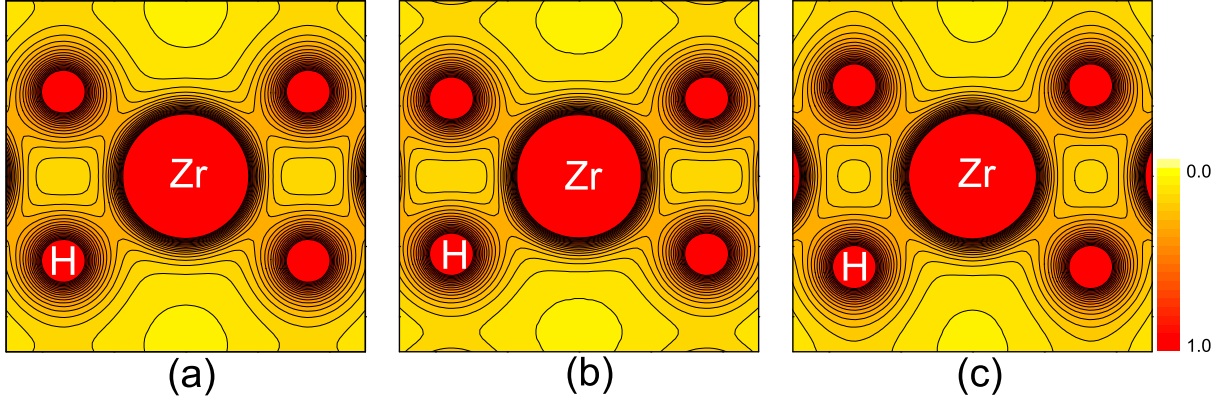


FIG. 4: Valence charge density of (a) fcc phase in (110) plane, (b) fct0.885 in (100) plane, and (c) fct1.111 in (100) plane. The contour lines are drawn from 0.0 to 1.0 at $0.05 e/\text{\AA}^3$ intervals.

in the vicinity of the Fermi level is caused by the splitting of the band in this region. As a consequence, the Fermi level in the two tetragonal phases is not located at a peak of the DOS but at a local minimum, which leads to a reduction in the electronic contribution to the total energy. This behavior has been referred to as a Jahn-Teller mechanism, as indicated by previous experiments and theoretical works [6, 12, 17, 18].

To analyze the ionic/covalent character of zirconium dihydride, in the following we will carefully investigate the valence charge density distribution. The calculated valence charge density maps of the fct ZrH_2 at $c/a=0.885$ and $c/a=1.111$ in (100) plane and fcc ZrH_2 in (110) plane are plotted in Fig. 4. Obviously, the charge densities around Zr and H ions are all near spherical distribution with slightly deformed towards the direction to their nearest neighboring atoms. Covalent bridges, which represent the bonding nature of Zr–H bonds, is clearly shown in Fig. 4. In Fig. 5, we plot the line charge density distribution along the nearest Zr–H bonds. Clearly, three line charge density curves vary in almost the same way along the Zr–H bonds. One can find a minimum value of charge density for each bond at around the bridge locus (indicated by the arrow in Fig. 5). These minimum values are listed in Table V. Although these values are much smaller than $0.7 e/\text{\AA}$ for Si covalent bond, they are prominently higher than $0.05 e/\text{\AA}$ for Na–Cl bond in typical ionic crystal NaCl. Therefore, there are weak but clear weights in Zr–H bonds in both fcc and fct phases of ZrH_2 .

In addition, we have performed the Bader analysis [19, 20] for the three typical ZrH_2 cells. The charge (Q_B) enclosed within the Bader volume (V_B) is a good approximation

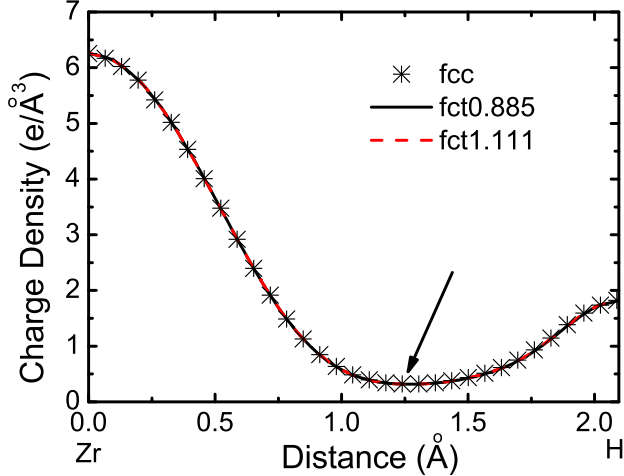


FIG. 5: The line charge density distribution between Zr atom and the nearest neighbor H atom for fcc, fct0.885, and fct1.111 structures of ZrH_2 .

to the total electronic charge of an atom. In this work, the default charge density grids for one primitive cell are $56 \times 56 \times 56$, $56 \times 56 \times 56$, $60 \times 60 \times 60$ for fcc, fct0.885, and fct1.111 cells, respectively. To check the precision, the charge density distributions are calculated with a series of n times finer grids ($n=2,3,4,5,6,7$). The deviation of the effective charge between the six and the seven times finer grids is less than 0.2%. Thus we perform the charge density calculations using the seven times finer grid ($392 \times 392 \times 392$, $392 \times 392 \times 392$, $420 \times 420 \times 420$) for fcc, fct0.885, and fct1.111 cells, respectively. The calculated results are presented in Table V. Note that although we have included the core charge in charge density calculations, only the valence charge are listed since we do not expect variations as far as the trends are concerned. From Table V, we find that the Bader charges and volumes for fcc and fct ZrH_2 are almost equal to each other. This shows similar ionic character, through a flux of charge (about 1.5 electrons for each Zr atom) from cations towards anions, for zirconium dihydride in their stable phase and metastable phases. The slight difference in charge distribution is mainly due to the structure distortion. Thus the ionicity of Zr-H bonds for ZrH_2 is also evident either for its fcc structure or fct structures.

C. Phonon dispersion curves

Phonon frequencies of the crystalline structure is one of the basic aspects when considering the phase stability, phase transformations, and thermodynamics of crystalline materials.

TABLE V: Calculated charges Q_B and volumes $V_B(\text{\AA}^3)$ according to Bader partitioning as well as the Zr–H distance (\AA) and relevant minimum values of charge densities ($e/\text{\AA}^3$) along the Zr–H bonds for ZrH_2 .

Compounds	$Q_B(\text{Zr})$	$Q_B(\text{H})$	$V_B(\text{Zr})$	$V_B(\text{H})$	Zr-H distance	Charge density _{min}
fcc	10.484	1.758	14.809	6.618	2.088	0.320
fct0.885	10.512	1.744	14.953	6.544	2.095	0.316
fct1.111	10.514	1.743	14.954	6.545	2.094	0.317

Employing the Hellmann-Feynman theorem [36, 37] and the direct method [38], we have calculated the phonon curves along some high symmetry directions in the BZ, together with the phonon DOS. For the phonon dispersion calculation, we use the $2 \times 2 \times 2$ fcc (fct) supercell containing 96 (48) atoms for fcc (fct) ZrH_2 and the $4 \times 4 \times 4$ Monkhorst-Pack k -point mesh for the BZ integration. In order to calculate the Hellmann-Feynman forces, we displace four and eight atoms, respectively, for fcc and fct ZrH_2 from their equilibrium positions and the amplitude of all the displacements is 0.03\AA . The calculated phonon dispersion curves along the Γ - X - K - Γ - L - X - W - L directions for fcc ZrH_2 and along the Γ - N - P - X - Γ - Z directions for fct ZrH_2 are displayed in Fig. 6. For both fcc and fct ZrH_2 , there are only three atoms in their primitive cell. Therefore, nine phonon modes exist in the dispersion relations. Due to the fact that zirconium is much heavier than hydrogen, the vibration frequency of zirconium atoms is apparently lower than that of hydrogen atoms. As a result, evident gap between the optic modes and the acoustic branches exists and the phonon DOS of fcc (fct) ZrH_2 can be viewed as two parts. One is the part lower than 7.4 (7.1) THz, where the main contribution comes from the zirconium sublattice, while the other part range from 30.7 to 37.9 (29.6 to 38.5) THz is dominated by the dynamics of the light hydrogen atoms. As shown by Fig. 6(b) and 6(c), all frequencies are positive for the two fct structures. This assures that the two fct phases are both dynamically stable. In contrast, one can see from Fig. 6(a) that the fcc phase of ZrH_2 is dynamically unstable. The transverse acoustic (TA) mode close to Γ point becomes imaginary along the Γ - K and Γ - L directions. The minimum of the TA branch locates at the Γ - K direction. Therefore, the fcc to fct phase transition probably can occur along the $[101]$ direction. This kind of dynamical instability of fcc phase compared to the stable fct phase is well consistent with our above-discussed mechanical stability analysis

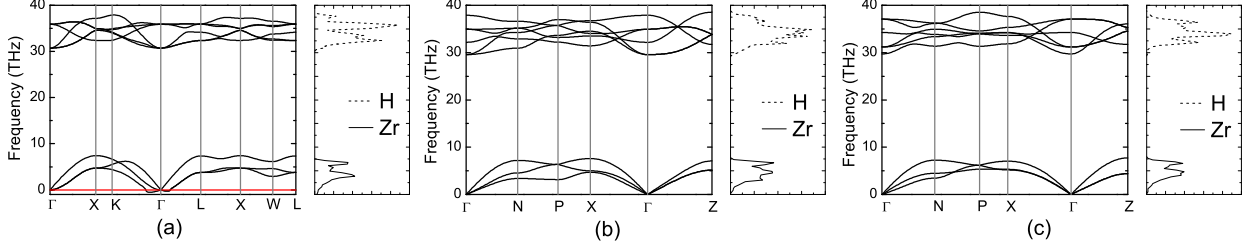


FIG. 6: Calculated phonon dispersion curves along the high-symmetry directions (left panel) and the corresponding PDOS (right panel) at ground state for (a) fcc ZrH_2 , (b) fct ZrH_2 at $c/a=0.885$, and (c) fct ZrH_2 at $c/a=1.111$.

of ZrH_2 .

IV. CONCLUSION

In summary, we have investigated the structural, mechanical, electronic, and thermodynamic properties of ZrH_2 in its stable and metastable phases by means of first-principles DFT-GGA method. Our optimized structural parameters are well consistent with previous experiments and theoretical calculations. Tetragonal distortion leads to bistable structures with $c/a > 1$ and $c/a < 1$, the latter of which corresponds to the experimentally observed low-temperature phase. Our total energy calculations illustrate that the most stable phase of ZrH_2 is the fct structure with $c/a=0.885$. Elastic constants, various moduli, Poisson's ratio, and Debye temperature are calculated for fcc and two fct phases of ZrH_2 . Mechanically unstable nature for fcc and fct1.111 structures are predicted. For fct0.885, mechanical stability and dynamical stability are firstly predicted by our elastic constants results and phonon dispersion calculation. The occupation characters of electronic orbital also accord well with experiments. Through Bader analysis, we have found that the Zr–H bonds exhibit weak covalent character while the ionic property is dominant with about 1.5 electrons transferring from each Zr atom to H. Our calculated phonon curves of fcc ZrH_2 have shown that the TA mode becomes imaginary close to Γ point along the $[101]$ direction.

V. ACKNOWLEDGMENTS

This work was partially supported by NSFC under Grants No. 90921003 and No. 60776063.

-
- [1] Y. Fukai, *Metal Hydrogen System. Basics Bulk Properties*, Springer, Berlin, 2005.
 - [2] P.W. Bickel, T.G. Berlincourt, *Phys. Rev. B* 2 (1970) 4807.
 - [3] L. Holliger, A. Legris, R. Besson, *Phys. Rev. B* 80 (2009) 094111.
 - [4] C.E. Ellis, *J. Nucl. Mater.* 28 (1968) 129.
 - [5] J. Huang, B. Tsuchiya, K. Konashi, M. Yamawaki, *J. Nucl. Sci. Technol.* 37 (2000) 887.
 - [6] J.H. Weaver, D.J. Peterman, D.T. Peterson, A. Franciosi, *Phys. Rev. B* 23 (1981) 1692.
 - [7] E. Zuzek, J.P. Abriata, A.S. Martin, F.D. Manchester, *Bull. Alloy Phase Diagrams* 11 (1990) 385.
 - [8] F. Ducastelle, R. Caudron, P. Costa *J. Physique* 31 (1970) 57.
 - [9] A.C. Switendick, *J. Less-Common Met.* 101 (1984) 191.
 - [10] G.J. Ackland, *Phys. Rev. Lett.* 80 (1998) 2233.
 - [11] H.L. Yakel, *Acta Crystallogr.* 11 (1958) 46.
 - [12] R.C. Bowman Jr., E.L. Venturini, B.D. Craft, A. Attalla, D.B. Sullenger, *Phys. Rev. B* 27 (1983) 1474.
 - [13] R.C. Bowman Jr., B.D. Craft, *J. Phys. C* 17 (1984) L477.
 - [14] R.C. Bowman Jr., B.D. Craft, J.S. Cantrell, E.L. Venturini, *Phys. Rev. B* 31 (1985) 5604.
 - [15] O.J. Zogal, B. Nowak, K. Niedzwiedz, *Solid State Commun.* 80 (1991) 601.
 - [16] K. Niedzwiedz, B. Nowak, O.J. Zogal, *J. Alloys Compd.* 194 (1993) 47.
 - [17] W. Wolf, P. Herzig, *J. Phys.: Condens. Matter* 12 (2000) 4535.
 - [18] R. Quijano, R. Coss, D.J. Singh, *Phys. Rev. B* 80 (2009) 184103.
 - [19] W.F.W. Bader, *Atoms in Molecules: A Quantum Theory*, Oxford University Press, New York, 1990.
 - [20] W. Tang, E. Sanville, G. Henkelman, *J. Phys.: Condens. Matter* 21 (2009) 084204.
 - [21] G. Kresse, J. Furthmüller, *Phys. Rev. B* 54 (1996) 11169.
 - [22] P.E. Blöchl, *Phys. Rev. B* 50 (1994) 17953.

- [23] J.P. Perdew, K. Burke, M. Ernzerhof, Phys. Rev. Lett. 77 (1996) 3865.
- [24] H.J. Monkhorst, J.D. Pack, Phys. Rev. B 13 (1972) 5188.
- [25] M. Methfessel, A.T. Paxton, Phys. Rev. B 40 (1989) 3616.
- [26] P.E. Blöchl, O. Jepsen, O.K. Andersen, Phys. Rev. B 49 (1994) 16223.
- [27] F. Birch, Phys. Rev. 71 (1947) 809.
- [28] J.F. Nye, Physical Properties of Crystals, Their Representation by Tensors and Matrices, Oxford Press, Chap.VIII, 1957.
- [29] J.H Westbrook, R.L Fleischer (Ed.), Intermetallic Compounds: Principles and Practice, Voll: principles, Wiley, London, 1995, Chap. 9, p. 195.
- [30] J.F. Nye, Physical Properties of Crystals, Oxford University Press, 1985.
- [31] W. Voigt, Lehrburch der Kristallphysik, Teubner,Leipzig, 1928.
- [32] A. Reuss, Z. Angew, Math. Mech. 9 (1929) 49.
- [33] R. Hill, Phys. Soc. London 65 (1952) 350.
- [34] O.L. Anderson, J. Phys. Chem. Solids 24 (1963) 909.
- [35] W. Liu, B. Li, L. Wang, J. Zhang, and Y. Zhao, J.Appl. Phys. 104 (2008) 076102.
- [36] O.H. Nielsen, R.M. Martin, Phys. Rev. B 32 (1985) 3780
- [37] O.H. Nielsen, R.M. Martin, Phys. Rev. B 35 (1987) 9308
- [38] K. Parlinski, Z.Q. Li, Y. Kawazoe, Phys. Rev. Lett. 78 (1997) 4063.